Airplane Recognition in TerraSAR-X Images via Scatter Cluster Extraction and Reweighted Sparse Representation

Zongxu Pan, Xiaolan Qiu, Zhongling Huang, and Bin Lei

***Abstract*— Target recognition in synthetic aperture radar (SAR) images has become a hotspot in recent years. The backscattering characteristic of target is a significant issue taken into consideration in SAR applications. Almost all of the previous work focus on the scatter point extraction to depict the backscattering characteristic of the target; however, a point-target corresponds to a region rather than a single point due to the convolution during the imaging. Based on this fact, we first analyze the extent to how a point-target spreads, then propose a novel scatter cluster extraction (SCE) method, and utilize the scatter cluster as the feature to solve the airplane recognition problem in SAR images. In practice, there often exist interfering objects near the target to be classified. To overcome this issue, we design a reweighted sparse representation (RSR)-based automatic purifying method by assigning a weight to each element of the feature iteratively according to the representation error. Since the element with large representation error always corresponds to the interfering objects, we give it a small weight, consequently suppressing the influence of the interference. Experimental results demonstrate that the proposed SCE method outperforms the traditional scatter point extraction-based method as well as some state-of-the-art methods. The comparison result also validates the effectiveness of the proposed RSR method.**

***Index Terms*— Airplane recognition, reweighted sparse representation (RSR), scatter cluster extraction (SCE), synthetic aperture radar (SAR) images.**

I. Introduction

SYNTHETIC aperture radar (SAR) is an effective earth observation system, which unlike optical systems, is not significantly affected by meteorological conditions. Target recognition in SAR images is a worth studying problem in the field of SAR application and has attracted a lot of interest recently.

As a hotspot, there have been some literature working on the target recognition in SAR images. Zhang *et al.* [1] classify three kinds of ships by analyzing the features of these ships. The constant false-alarm rate (CFAR) algorithm is used to extract the scatter points of the target and the identity of a query ship is obtained through a decision tree designed for the three kinds of ships. In [2], the geometric information together with the density of the radar cross section (RCS) of ships is extracted as the feature. Then the sparse representation classifier (SRC) is used to obtain the identity of the target. We denote this method as the SRC method. Zhang *et al*. [3] propose a kernel SRC (KSRC)-based method, in which KSRC rather than the traditional SRC is applied. The Gabor-support vector machine (SVM) method for SAR target recognition is proposed in [4], in which Gabor filter is used to extract the feature and SVM is applied as the classifier. As sample numbers are usually inadequate for target recognition in SAR images, the study in [5] utilizes the simulated images to train the classifier and use the real images to test. Hu's invariant moments are used in [6] to extract the stable feature of the target and SVM is applied as the classifier. Chen *et al*. [7] utilize corner detectors to extract the salient points vector (SPV) of the airplane, and recognize the target via template matching.

In this letter, we propose a target recognition method in SAR images via scatter cluster extraction (SCE) and reweighted sparse representation (RSR), and apply the method to airplane recognition in TerraSAR-X images. Specifically speaking, three types of airplanes, B52, B707, and straight wing (SW) airplanes shown in Fig. 1 are used as the targets. The target recognition problem is not at all straightforward as two targets belonging to the same category may vary a lot when their incidence or azimuth angles differ. It is indicated in [8] that in high-resolution SAR images, the RCS of the target is mainly determined by the geometric structure of its subcomponents, and the subcomponents of the target will form strong scatter points. Consequently, almost all of the previous work emphasizes the extraction of the scatter point, such as CFAR and SPV detection. However, according to the imaging theory of SAR, a point-target corresponds to a region rather than a single point in the image due to the convolution during the imaging. In this letter, we refer to the backscattering region of the point-target or the subcomponents of the target as scatter cluster. It is apparent that extracting the scatter cluster to describe the characteristic of the target is more reasonable. On the other hand, most of the literature focuses on the case when there are no or few interfering objects near the target to be classified or when the image is purified manually

Manuscript received June 13, 2016; revised September 16, 2016 and October 20, 2016; accepted November 7, 2016. This work was supported in part by the National Natural Science Foundation of China under Grant 61331017 and in part by the Major Project of High Resolution Earth Observation System under Grant 30-Y20A12-9004-15/16.

The authors are with the Key Laboratory of Technology in Geo-spatial Information Processing and Application System, Institute of Electronics, Chinese Academy of Sciences, Beijing 100190, China (e-mail: zxpan@mail.ie.ac.cn).

Color versions of one or more of the figures in this letter are available online at http://ieeexplore.ieee.org.

Digital Object Identifier 10.1109/LGRS.2016.2628162

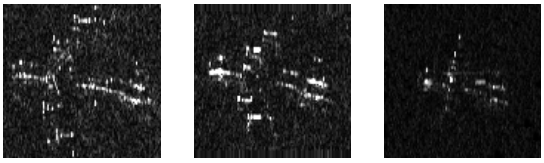

Fig. 1. Three types of airplanes in TerraSAR-X images. B52 (left), B707 (middle), and SW (right).

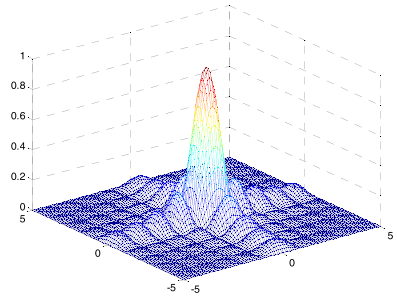

Fig. 2. Absolute of the 2-D sinc function.

in advance. However, in the real application, there always exist interfering objects near the target, making the background complex and so increasing the difficulty of the problem. To overcome this issue, we design an RSR-based automatic purifying method by assigning a weight to each element of the feature iteratively according to the representation error. As the element with large representation error always corresponds to the interfering objects, we give it a small weight, consequently suppressing the influence of the interfering objects.

The remainder of this letter is organized as follows. Section II analyzes the scatter cluster of the target in SAR images and details how to extract the scatter cluster. In Section III, an airplane recognition method via SCE and RSR is proposed. The experimental results are shown in Section IV and the conclusions are given in Section V.

II. Scatter Cluster Extraction

In this section, we first analyze the backscattering properties of SAR targets, and then detail the proposed SCE method. SAR target consists of a set number of subcomponents, each of which can be viewed as a combination of several point-targets. Ideally, a point-target corresponds to a single point in the image, however, due to the convolution during the imaging, the point will be diffused in the image. Suppose there is a point-target located in (m, n) with intensity I, then it can be written as $I\delta\ (i-m, j-n)$, where $\delta\ (i, j)$ is the 2-D Dirichlet function. After the convolution, it will change to $I|\mathrm{Sinc}(i-m, j-n)|$, where $\mathrm{Sinc}(i, j) = ((\sin \pi ai)/(\pi ai))((\sin \pi bj)/(\pi bj))$ is the 2-D sinc function. The coefficients a and b are determined by imaging parameters, satisfying $a = B_s/f_s$ and $b = B_a/f_p$, where B_s, f_s, B_a, and f_p are the bandwidth of the signal, sampling frequency, processing bandwidth, and pulse repetition frequency. Fig. 2 plots the absolute value of $\mathrm{Sinc}(i, j)$, and the intensity of the first sidelobe is -13.26 dB, that is, 0.2173 of the maximum value in magnitude. It is worth noting that the decrement of the first sidelobe is independent of the parameters a and b.

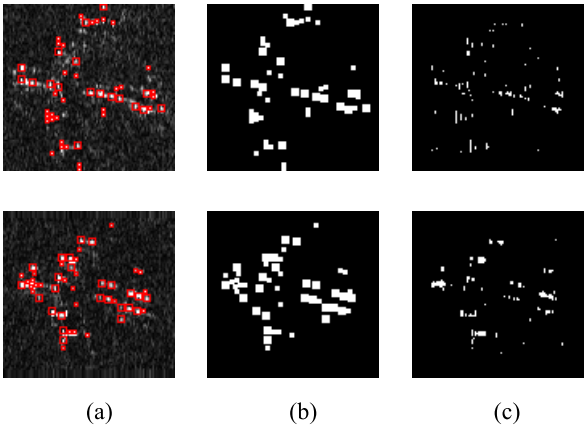

Fig. 3. Comparison results of SCE and CFAR for a B52 (top) and a B707 (bottom) airplane. (a) SCE results. (b) Binary images obtained via SCE. (c) Binary images obtained via CFAR.

The principle of SCE is based on the fact that the center of the cluster should be a peak point that is surrounded by several points with decreased intensity. For a peak pixel x_p, to obtain the cluster it belongs to, search the points x surrounding it, if the intensity ratio between x and x_p is larger than a preset value τ, then x is treated as the point in the cluster. τ can be set to 0.2173, which is the intensity ratio between the sidelobe and the peak point. In order to make the SCE result more robust, two more constraints are added to the method. One constraint is that if a peak value is already in one cluster, it will not be considered as the center point in any other clusters. The other constraint is that the radius of the cluster should not be too small, in which case, the points in that cluster are likely to be the points with strong intensity caused by noise. Based on the above analysis, we proposed a seed-growing-based SCE method that consists of the following four steps.

1) *Step 1:* Set the parameters used in SCE, that is, the number of clusters N, the minimum intensity ratio τ, and the minimum radius of clusters $r_{\min}$.
2) *Step 2:* Sort pixels of the image in descending order and take out the points one by one as the seed point when the number of clusters is less than N.
3) *Step 3:* For a seed point, if the point is already in a certain cluster, take the next point, otherwise, set the current radius of the cluster r at 0, then gradually increase the radius of the cluster and calculate the mean intensity of the pixels in the circle with radius r until the ratio between the mean intensity and the intensity of the seed point is less than τ.
4) *Step 4:* If the radius of the cluster is not smaller than $r_{\min}$, set all the points in the cluster as the scatter points and go to Step 3 to process the next point until the number of clusters is up to N.

Fig. 3 shows the SCE results of a B52 and a B707, and compares the binary images obtained via SCE and CFAR. As illustrated in Fig. 3, after SCE the noise can be removed markedly; in the meanwhile the shape of the target is reserved. It is also indicated from Fig. 3 that SCE has better ability to extract scatter points than CFAR, which is a point extraction-based method.

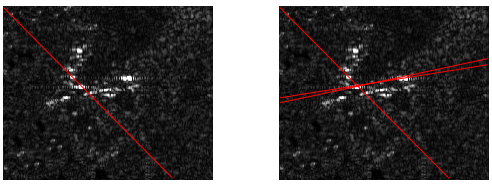

(a) (b)

Fig. 4. Principal direction extraction through HT. (a) Detect one line using HT. (b) Detect three lines using HT.

III. Airplane Recognition via SCE and RSR

A. Preprocessing

Before recognizing the target, we should align the image first. Hough transform (HT) [9] is used to extract the principal axis of the target. HT tends to be affected by strong points, Fig. 4(a) for example. To solve this problem, we detect several lines, as shown in Fig. 4(b), and find the two closest lines in terms of the angle of the line. The mean angle of the two lines is looked upon as the principal direction of the target. Then the image is rotated accordingly and by scanning each line of the rotated image, we can get the principal axis of the target. Finally, by searching the first and the last bright points along the principal axis, we can obtain the head and the tail of the airplane. Here, bright points are defined as the points whose intensity is larger than $\tau_m x_m$, where x_m is the maximum value of the image and τ_m is a preset parameter. We add a constraint that the first and the last bright points should be surrounded by other bright points to reduce the influence of noise. When the head and the tail of the airplane are determined, the central point can be obtained and the images are aligned according to the central point.

B. Airplane Recognition Through Reweighted Sparse Representation

The aligned binary image is divided into blocks and the density of scatter points in each block is concatenated to form the feature. The SCE feature has the following two advantages.

1) The feature provides not only density but also position information of the scatter point, therefore, although roughly, it reflects the topology of scatter clusters of the target, which is significant for target recognition in SAR images.
2) The feature is insensitive to image misalignment, which is inevitable in a real application.

As suggested from the recent research in the pattern recognition field, SRC is an effective classifier and has been widely used in many classification problems. We will briefly introduce SRC first, and then detail the proposed RSR method. Denote by $\mathbf{X}_k$ the training data set of the kth category, and each column of $\mathbf{X}_k$ is one training sample in the kth category; here the training sample refers to the image stacked as a vector or the feature extracted from the image. Suppose there are K categories to be classified, let $\mathbf{X} = [\mathbf{X}_1 \dots \mathbf{X}_K]$ be the whole training data set. SRC codes the query data $\boldsymbol{y}$ over $\mathbf{X}$ by solving the following ℓ_1-norm minimization problem first:

$$\hat{\boldsymbol{\alpha}} = \arg\min_{\boldsymbol{\alpha}} \left\{ \|\boldsymbol{y} - \boldsymbol{X}\boldsymbol{\alpha}\|_2^2 + \lambda \|\boldsymbol{\alpha}\|_1 \right\} \tag{1}$$

where $\boldsymbol{\alpha}$ is the representation coefficient and λ is the Lagrangian factor that balances the tradeoff between the fidelity and the sparsity terms. Equation (1) is essentially a sparsity constrained convex optimization problem that searches $\boldsymbol{\alpha}$ to make $\boldsymbol{y} \approx \boldsymbol{X}\boldsymbol{\alpha}$ and in the meantime to make $\boldsymbol{\alpha}$ as sparse as possible with respect to ℓ_1-norm. $\hat{\boldsymbol{\alpha}}$ can be written as $\hat{\boldsymbol{\alpha}} = [\hat{\boldsymbol{\alpha}}_1; \dots; \hat{\boldsymbol{\alpha}}_K]$, where $\hat{\boldsymbol{\alpha}}_k$ is the coefficient corresponding to the kth category. Then SRC computes the representation residual of each category as follows:

$$\epsilon_k = \|\boldsymbol{y} - \mathbf{X}_k \hat{\boldsymbol{\alpha}}_k\|_2 \tag{2}$$

and the identity of the query data $\boldsymbol{y}$, denoted by $k_{\boldsymbol{y}}$, is obtained by finding the category that can represent $\boldsymbol{y}$ with the minimum residual, that is

$$k_{\boldsymbol{y}} = \arg\min_k \{\epsilon_k\}. \tag{3}$$

It is known that only when the error $\boldsymbol{e} = \boldsymbol{y} - \mathbf{X}\boldsymbol{\alpha}$ obeys the Gaussian distribution, the solution of (1) is the maximum likelihood estimation solution of the problem. However, usually $\boldsymbol{e}$ does not meet this condition in practice, especially when there are interfering objects near the target, as some elements of $\boldsymbol{e}$ will become very large, and in this case the recognition rate of SRC will decrease because SRC does not take the issue into account. Although one can use the data with interfering objects as the training sample, the improvement is not obvious as the position of the interfering object is completely random. In order to reduce misclassification resulting from the interfering objects, we design an RSR automatic purifying method by assigning each element e_i of $\boldsymbol{e}$ with a weight w_i. As e_i with a large value often corresponds to the region having interfering objects, we assign it with a small weight w_i. Define a diagonal matrix $\mathbf{W}$ whose diagonal element is the weight w_i, $i = 1, \dots, n$, then the RSR method can be formulated as solving the following optimization problem:

$$\hat{\boldsymbol{\alpha}} = \arg\min_{\boldsymbol{\alpha}} \left\{ \|\mathbf{W}(\mathbf{y} - \mathbf{X}\boldsymbol{\alpha})\|_2^2 + \lambda \|\boldsymbol{\alpha}\|_1 \right\} \tag{4}$$

where w_i satisfies

$$w_i = f_u\left(\frac{2\exp\left(-e_i^2/h\right)}{1 + \exp\left(-e_i^2/h\right)} \right) \tag{5}$$

where h is a constant and $f_u(x)$ is a thresholding function with parameter u defined as follows:

$$f_u(x) = \begin{cases} x, & x \geq u \\ 0, & x < u. \end{cases} \tag{6}$$

We initialize $\mathbf{W}$ with the identity matrix, that is, $\mathbf{W}^{(0)} = \mathbf{I}$, and then iteratively update the weight matrix $\mathbf{W}$ and the representation coefficient $\boldsymbol{\alpha}$. Suppose after t iterations the weight matrix is $\mathbf{W}^{(t)}$, then by solving (4) we can obtain the representation coefficient $\hat{\boldsymbol{\alpha}}^{(t)}$. Therefore, the error $\boldsymbol{e}^{(t)}$ can be calculated through $\boldsymbol{e}^{(t)} = \boldsymbol{y} - \mathbf{X}\hat{\boldsymbol{\alpha}}^{(t)}$, then w_i is reweighted via (5) to get $\mathbf{W}^{(t+1)}$. This process is repeated until the change of $\mathbf{W}$ between two adjacent iterations is small enough or t reaches the number of iterations. To explain why RSR works, let us look at the first term of the object function in (4). If we rewrite $\mathbf{W}\boldsymbol{y}$ as $\boldsymbol{y}'$ and $\mathbf{W}\mathbf{X}$ as $\mathbf{X}'$, (4)

has the same form as (1) and the difference lies in that $\boldsymbol{y}$ is reweighted using $\mathbf{W}$. When e_i is very small, w_i approximates one, therefore y_i' in $\boldsymbol{y}'$ is nearly equal to y_i; and when e_i is large which often corresponds to the region with interfering objects, w_i is less than one, consequently the corresponding element y_i' is smaller than y_i because $y_i' = w_i y_i$. In RSR, the larger the representation error e_i is, the smaller the element y_i' becomes; therefore, the RSR method has the ability to reduce the influence of the interfering objects. The above fact can be seen more clearly by expanding $\|\mathbf{W}(\boldsymbol{y} - \mathbf{X}\boldsymbol{\alpha})\|_2^2$ as $\sum_i w_i^2(y_i - \boldsymbol{x}_i^T\boldsymbol{\alpha})^2$, where $\boldsymbol{x}_i^T$ is the ith row of $\mathbf{X}$. It is obvious that y_i with a small w_i plays a less role in the object function benefiting from the reweighted operation. When the iteration terminates, we can use (2) and (3) to obtain the identity of the query target. A better scheme is training an SVM classifier using the training data and making $\boldsymbol{y}' = \mathbf{W}^{(T)}\boldsymbol{y}$ as the test data, where $\mathbf{W}^{(T)}$ is the weight matrix when the iteration terminates. As SVM has excellent ability for problem with small sample size and $\boldsymbol{y}'$ obtained through RSR method can be seen as a purified version of $\boldsymbol{y}$, it can achieve better recognition result.

IV. Experimental Results and Discussion

To validate the effectiveness of the proposed method, several experiments are conducted on four HH-polarized TerrarSAR-X spotlight amplitude images of the aircraft boneyard in Davis. The incidence angles of the four images are 45.1°, 45.2°, 45.1°, and 41.3°, respectively, and the spatial resolution is 0.5 m × 0.5 m. We manually collect two airplane data sets from the four images. Data set I consists of 125 B52, 129 B707, and 134 SW airplanes, and we manually remove apparent interfering objects if they exist. Data set II consists of 10 B52, 10 B707, and 10 SW airplanes with severe interfering objects. The lengths of B52, B707, and SW are 48.5, 46.61, and 34 m, and the width of their wings are 56.4, 44.42, and 22 m, respectively. The selected targets consist of 128 × 104 pixels.

When using the SCE feature, there are three schemes to obtain the identity of the target. We denote the method using SVM classifier as SCE-SVM, using RSR to purify the data followed by SRC as SCE-RSR-SRC, and using RSR to purify the data followed by SVM classifier as SCE-RSR-SVM. We compare these three methods with the principal component analysis (PCA)-SVM method, the CFAR-SVM method, the SRC method in [2], the KSRC method in [3], the Gabor-SVM method in [4], and the SPV method in [7] on data set I. The parameters in the proposed method are set as follows: N is set to 50, τ is set to 0.3, $r_{\min}$ is set to 1, τ_m is set to 0.5, and M is set to 64. For SCE-RSR-SRC and SCE-RSR-SVM, we use the ℓ_1-ls method [10] to solve the ℓ_1–norm minimization problem and the number of iterations is set to 10. We randomly select p percent samples of data set I as the training data and take the remainder samples as the testing data. To decrease the influence of the sample selection, the experiment is conducted several times and we take the average recognition rate as the final result. Table I lists the recognition rates of various methods and the average runtimes of PCA-SVM, CFAR-SVM, SRC, KSRC, Gabor-SVM, SPV, SCE-SVM, SCE-RSR-SRC, and SCE-RSR-SVM are 0.52, 624.82, 160.03, 72.37, 355.2, 124.66, 7.09, 176.94, and 180.30 ms, respectively. The experimental results show the following.

TABLE I
Comparison of Recognition Rates (%) of Different Methods

p	0.05	0.1	0.2	0.3
PCA-SVM	70.73	79.94	89.35	89.67
CFAR-SVM	79.13	87.97	89.03	92.99
SRC[2]	79.40	85.67	86.45	88.56
KSRC[3]	85.91	94.27	94.19	95.94
Gabor-SVM[4]	90.24	94.27	95.48	96.31
SPV[7]	86.18	91.40	95.48	94.46
SCE-SVM	86.72	95.13	96.13	97.05
SCE-RSR-SRC	83.74	88.25	93.23	94.83
SCE-RSR-SVM	91.87	95.42	97.10	97.79

TABLE II
Recognition Rates (%) of SCE-RSR-SVM With Various τ

τ	0.1	0.2	0.3	0.4	0.5
Recognition rate	96.45	96.77	97.10	96.13	96.13

1) The proposed SCE-based methods outperform the traditional PCA and CFAR-based methods, which validates the effectiveness of the SCE feature.
2) The SCE-RSR-SVM method achieves the best recognition rate and by further analyzing the probably confusion matrix of each method, we can see that compared with the other methods, SCE-RSR-SVM has better ability to distinguish between B52 and B707, and in the meantime is competitive for recognizing the SW airplanes.
3) SCE-RSR-SVM outperforms SCE-RSR-SRC, and the reason is partly that SRC needs a certain amount training data to get a satisfactory result; however, even when p is set to 0.3, the number of the training data is still small. It can be noticed that with the increase of p, the gap in recognition rates between SCE-RSR-SRC and SCE-RSR-SVM reduces.
4) SCE-RSR-SVM is better than SCE-SVM, which demonstrates that RSR is an effective tool to purify the data.

To see how parameter τ affects the proposed method, we set τ to different values and the recognition rates of SCE-RSR-SVM with various τ are shown in Table II. It is indicated that the optimal τ in the experiment is 0.3, and too small or too large a value of τ will both decrease the recognition rate. The incidence and azimuth angles play a key role in SAR target recognition. To discuss the effect of the incidence and azimuth angles on the proposed method, we conduct the following experiment. First, we divide data set I into two parts S1 and S2 according to the incidence angle, and samples having similar incidence angles are grouped into one set. Then part of samples in S1 are selected to form the training set, the remaining samples in S1 are taken as the testing set S1, and samples in S2 are taken as the testing set S2. Therefore, the samples in S1 and the training set have similar incidence angles while the incidence angles of the samples in S2 and the training set are quite different. Table III lists the recognition rates of SCE-RSR-SVM on S1 and S2. It can be

TABLE III
RECOGNITION RATES (%) OF SCE-RSR-SVM ON S1 AND S2

	B52	B707	SW	Total
S1	100	98.53	96.47	97.75
S2	84.62	97.14	68.18	85.71

TABLE IV
RECOGNITION RATES (%) OF SCE-RSR-SVM ON T1 AND T2

	B52	B707	SW	Total
T1	100	88.24	100	96.88
T2	81.08	77.05	91.18	81.82

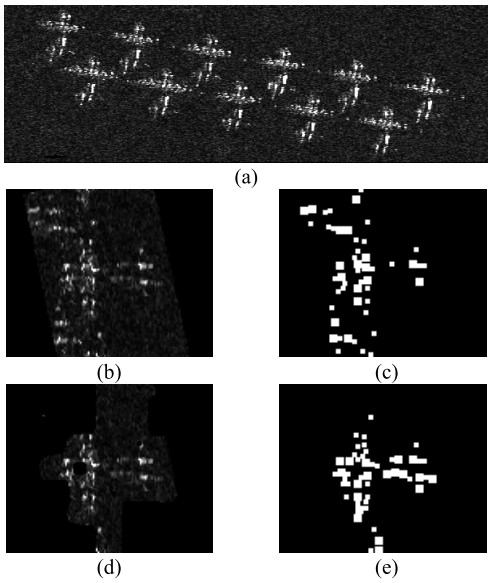

Fig. 5. Comparison of the image and SCE results before and after reweighting. (a) Image having close targets. (b) Image slice before reweighting. (c) SCE result of (b). (d) Image slice after reweighting. (e) SCE result of (d).

seen from Table III that when the incidence angles of the training and the testing data are quite different, the performance of the approach will decrease evidently. A similar experiment is conducted to reveal the influence of the azimuth angle. In the experiment, data set I is divided into the training set and the testing sets T1 and T2. The samples in T1 and the training set have similar azimuth angles while the azimuth angles of the samples in T2 and the training set are quite different. The experimental result shown in Table IV indicates that when the azimuth angles of the training and the testing data are quite different, the performance of the approach will decrease evidently.

As mentioned in Section III, SCE-RSR-SVM would have more advantages when the image has severe interfering objects. To validate this, we conduct another set of experiments, in which 30% samples of data set I are used as the training data and the samples in data set II are taken as the testing data. Since it is hard to find the major direction of the target when the interference is severe, we manually align the testing data. The recognition rate of SCE-SVM and SCE-RSR-SVM are 73.33% and 80%, respectively, and the result indicates that SCE-RSR-SVM has more advantages than SCE-SVM when the data have interfering objects, recalling that in the first set of experiment the two methods have similar performances when $p = 0.3$. Fig. 5 illustrates why RSR works when dealing with an image having interfering objects. Fig. 5(a) is an image having close targets, therefore when we cut the image slice from this image, there will be severe interfering objects near the target in the image slice as shown in Fig. 5(b). Fig. 5(c) is the SCE result of Fig. 5(b). It is apparent that when directly using Fig. 5(c) as the feature, neither SVM nor the SRC can obtain the correct result. Fig. 5(d) and (e) gives the reweighted image and the corresponding SCE result. It can be seen clearly that most of the interfering objects are removed through reweighting in RSR, so a correct result can be obtained.

V. CONCLUSION

An SCE and RSR-based method for airplane recognition is proposed in this letter. The feature obtained via SCE can better depict the characteristic of the target than that obtained through the traditional point extraction-based method, as a point-target corresponds to a region in the image due to the convolution process in the imaging. We then design an RSR-based automatic purifying method by assigning a weight to each element of the feature iteratively according to the representation error. The experimental results demonstrate the effectiveness of the SCE feature and the RSR method, especially when the data are affected by interfering objects. In addition, the proposed method can be generalized to other recognition problems in SAR images without major modification.

REFERENCES

[1] H. Zhang, X. Tian, C. Wang, F. Wu, and B. Zhang, "Merchant vessel classification based on scattering component analysis for COSMO-SkyMed SAR images," *IEEE Geosci. Remote Sens. Lett.*, vol. 10, no. 6, pp. 1275–1279, Nov. 2013.

[2] X. Xing, K. Ji, H. Zou, W. Chen, and J. Sun, "Ship classification in TerraSAR-X images with feature space based sparse representation," *IEEE Geosci. Remote Sens. Lett.*, vol. 10, no. 6, pp. 1562–1566, Nov. 2013.

[3] L. Zhang, Z. Tao, and B. Wang, "SAR image target recognition using kernel sparse representation based on reconstruction coefficient energy maximization rule," in *Proc. IEEE ICASSP*, Shanghai, China, Mar. 2016, pp. 2369–2373.

[4] F.-M. Hu, P. Zhang, R. Yang, and X. Fan, "SAR target recognition based on Gabor filter and sub-block statistical feature," in *Proc. IET Int. Radar Conf.*, Guilin, China, Apr. 2009, pp. 1–4.

[5] Y. L. Chang, C. Y. Chiang, and K. Chen, "SAR image simulation with application to target recognition," *Prog. Electromagn. Res.*, vol. 119, no. 4, pp. 35–57, 2011.

[6] Y. Fu, W. Mei, and Z. Chunqin, "SAR image target recognition based on Hu invariant moments and SVM," in *Proc. 5th Int. Conf. Inf. Assurance Secur.*, vol. 1. Xian, China, Aug. 2009, pp. 585–588.

[7] J. Chen, B. Zhang, and C. Wang, "Backscattering feature analysis and recognition of civilian aircraft in TerraSAR-X images," *IEEE Geosci. Remote Sens. Lett.*, vol. 12, no. 4, pp. 796–800, Apr. 2015.

[8] J. A. Jackson and R. L. Moses, "Synthetic aperture radar 3D feature extraction for arbitrary flight paths," *IEEE Trans. Aerosp. Electron. Syst.*, vol. 48, no. 3, pp. 2065–2085, Jul. 2012.

[9] J. Cha, R. H. Cofer, and S. P. Kozaitis, "Extended Hough transform for linear feature detection," *Pattern Recognit.*, vol. 39, no. 6, pp. 1034–1043, Jun. 2006.

[10] S.-J. Kim, K. Koh, M. Lustig, S. Boyd, and D. Gorinevsky, "An interior-point method for large-scale ℓ_1-regularized least squares," *IEEE J. Sel. Topics Signal Process.*, vol. 1, no. 4, pp. 606–617, Dec. 2007.